Textures and Microstructures, 1988, Vols. 8 & 9, pp. 443–456
Reprints available directly from the publisher
Photocopying permitted by license only

Printed in the United Kingdom

Texture Analysis by TOF Measurements of Spallation Neutrons with a 2D-Position Sensitive Detector

HANS-RUDOLF WENK

Department of Geology and Geophysics, University of California, Berkeley, CA 94720, USA

and

PHILLIP J. VERGAMINI and ALLEN C. LARSON

LANSCE, Los Alamos National Laboratory, Los Alamos, NM 87545, USA

(Received July 3, 1987)

Dedicated to the memory of Professor Günter Wassermann

A new method is introduced to measure preferred crystallographic orientation in deformed polycrystals. A pulsed beam of protons is accelerated in the linear accelerator at Los Alamos. The beam is then compressed in time in a storage ring and directed towards a W spallation target producing bursts of pulsed neutrons of 0.25 μs duration. The neutron beam (10^7 n cm^{-2} s^{-1}) is scattered by the polycrystal sample and diffractions, including time of flight of neutrons, are recorded on a 2D detector. This offers both simultaneous coverage of a wide d spectrum (many peaks) and a large orientation region (pole figure segment). Results on Al polycrystals obtained with this instrument agree well with pole figures measured by conventional X-ray diffraction.

KEY WORDS: Neutron diffraction, spallation source, time of flight method, 2D-detector, pole figure measurement.

INTRODUCTION

With the exception of some early studies (Brockhouse 1953, Betzl Kleinstück 1961), neutron diffraction has almost exclusively been

reserved for crystallographers for the investigation of crystal structures. Recently, however, there has been increasing interest in using this technique to determine crystallographic preferred orientation in polycrystals. A major advantage of neutrons compared to X-rays is their low absorption, which enables one to use large specimens (1–5 cm cubes or spheres) of coarse grainsize and to obtain good grain statistics and complete pole figures (Feldmann *et al.* 1980, Wenk *et al.* 1984). Application of position sensitive detectors (Bunge *et al.* 1982, Wenk *et al.* 1986) and pulsed neutron sources (Feldmann *et al.* 1980, Betzl *et al.* 1984) has added new possibilities for fast and accurate determination of the orientation distribution. In this paper we explore a combination of time-of-flight (TOF)

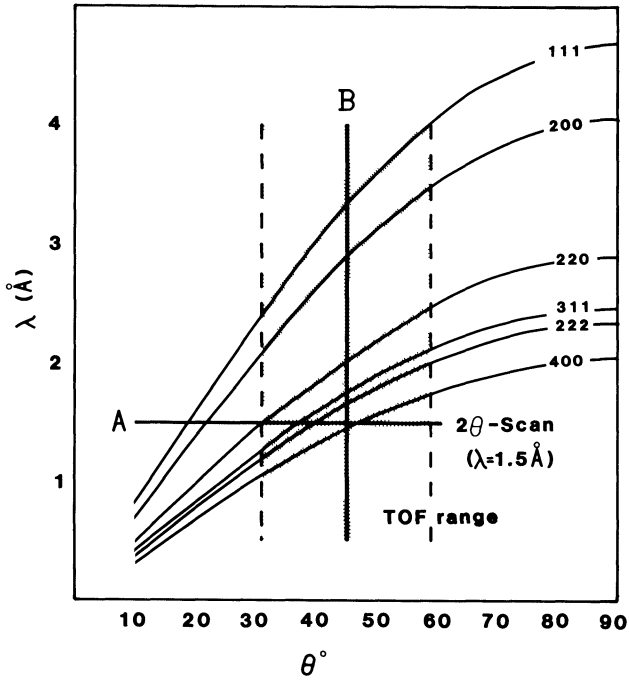

Figure 1 Bragg's law for low order diffractions of aluminum. (A) illustrates a 2Θ scan with a conventional goniometer and monochromatic radiation. (B) gives the coverage of a continuous spectrum at a fixed detector position. With a 2Θ position sensitive detector a large 2Θ and λ range is measured simultaneously (shaded area).

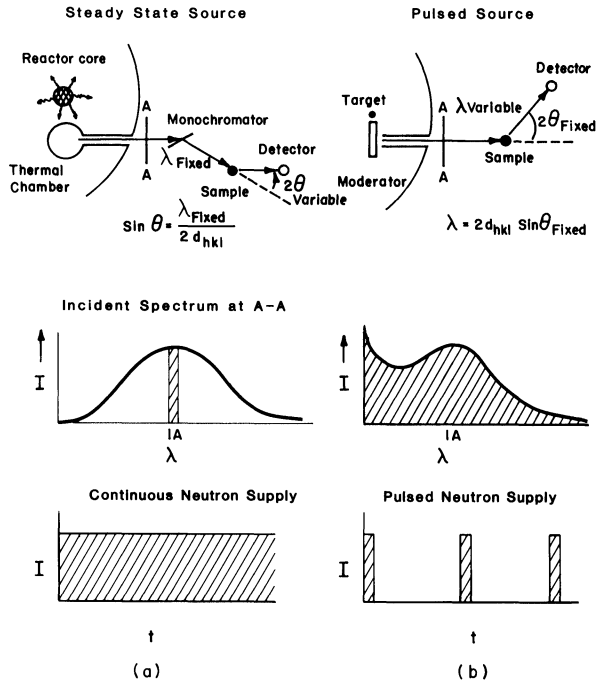

Figure 2 Comparison of a conventional neutron diffraction experiment with a continuous neutron supply (a) and TOF experiment with pulsed neutrons (b). Geometry of the experiments is shown on top, a typical spectrum in the center and the time variation of the flux at the bottom.

measurements of pulsed neutrons and two-dimensional position sensitive detectors for texture analysis of deformed materials, specifically, a sample of recrystallized aluminum.

Figure 1 displays Bragg's law for relevant reflections of aluminum. In a conventional experiment with monochromatic neutrons we scan the spectrum by moving the detector over the 2Θ range (Figure 2a and A in Figure 1). With a 1D-position sensitive detector set up along Θ, the whole spectrum can be covered at once. The diffraction spectrum can also be covered by TOF measurements of polychromatic neutrons at a fixed 2Θ angle (Figure 2b and B in Figure 1). Combining a 2D position sensitive detector with TOF, we not only get 2Θ resolution, but cover a large, three-dimensional

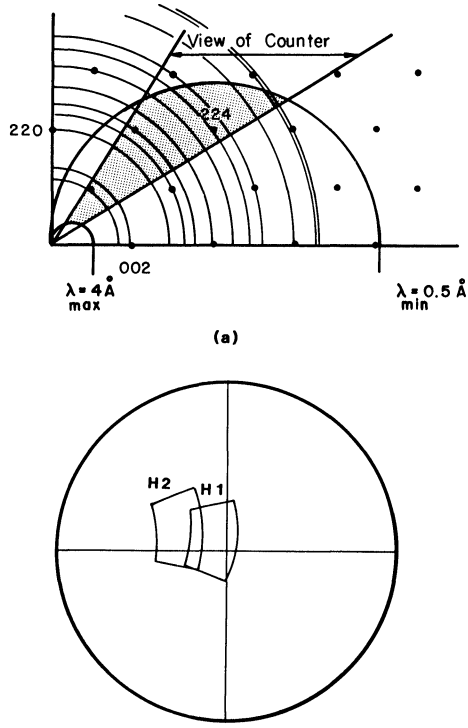

Figure 3 (a) Section of the reciprocal lattice for aluminum. The spheres of reflections for λ_{max} and λ_{min} are indicated. With a position sensitive detector and TOF analysis a whole range of orientations and d-spacings can be recorded simultaneously (shaded area). (b) Range of orientations for a typical detector and sample setting represented in equal area projection. Histogram 1: H1; histogram 2: H2.

sector of reciprocal space simultaneously, without requiring specimen rotations (shaded area in Figure 1).

Figure 3a illustrates an *hkl* section of reciprocal space for an aluminum single crystal with reflection *hkl* represented as spots diffracting with different intensity due to the corresponding structure factor. These intensities are used by crystallographers to

determine the crystal structure. The diffracting region between minimum and maximum wavelength λ is indicated. For a powder, the reciprocal lattice degenerates into a set of concentric shells with uniform surface occupancy. The reciprocal lattice of a polycrystal with texture is a set of spheres with variable surface occupancy. The density distribution on each *hkl* surface is a pole figure. With a position sensitive detector we can measure a sizable sector of many pole figures at once, as indicated by the shaded area. A sector for two typical detector and sample orientations is shown in Figure 3b in equal area projection. To cover a different sector of the pole figure requires a rotation of the polycrystalline specimen or of the detector into another orientation.

EXPERIMENTAL PROCEDURES

The general geometry of the neutron production facility is illustrated in Figure 4. A pulsed beam of H^{-1} is accelerated to 800 MeV in a linear accelerator at the Los Alamos Meson Physics Facility (LAMPF). This beam is stripped of electrons and the resulting

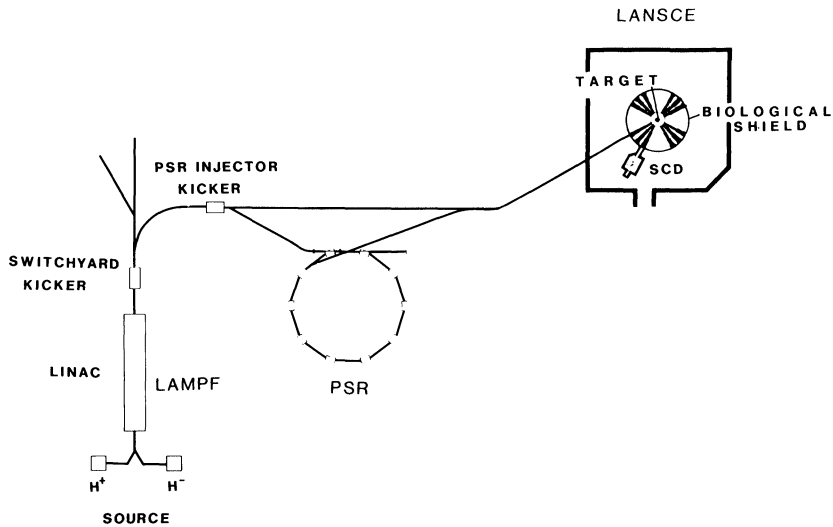

Figure 4 Ray path at the Los Alamos LAMPF, PSR, and LANSCE facilities. Linear accelerator: LINAC: proton storage ring: PSR; single crystal diffractometer: SCD.

proton beam injected into a Proton Storage Ring (PSR) where the pulse is compressed in time and then directed to the Los Alamos Neutron Scattering Center (LANSCE) spallation target. When these high energy protons, in 0.25 μs long pulses at a 12 Hz frequency, strike the tungsten target, a burst of high energy spallation neutrons is produced; these are moderated in hydrogenous material and collimated along time-of-flight paths for use in several experimental stations. (For details about the moderator, see Russel *et al.*1981). The experiments described here were carried out at the LANSCE Single Crystal Diffractometer (SCD).

The neutron pulse, generated at the target/moderator, propagates 7.5 m to the sample as a spectral wave front with the highest energy (short wavelength) neutrons arriving first as is illustrated in Figure 5, and the longer wavelengths arriving later. From this broad

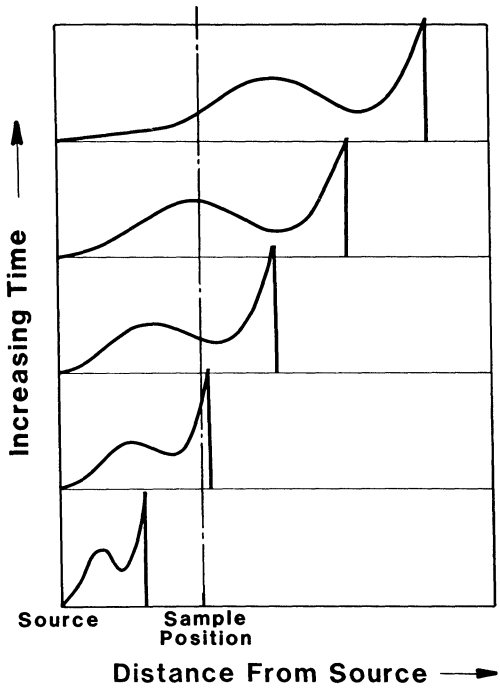

Figure 5 Propagation and distribution of a neutron pulse with time. The maximum wavelength which can be measured depends on the interval between pulses.

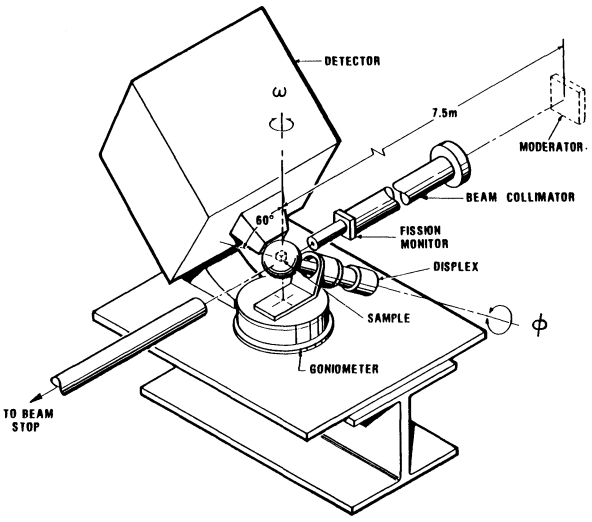

Figure 6 Schematic diagram illustrating the experimental setup at LANSCE-SCD. The sample is mounted on a two-circle goniometer. The detector axis is at 90° to the incoming beam.

spectrum a usable wavelength range is chosen (typically 0.5 to 4.0 Å, but it can be extended to 10 Å). The time averaged beam intensity at the sample is presently about 1×10^7 neutrons $cm^{-2} s^{-1}$, which compares favorably with other facilities where texture measurements have been done (conventional reactor, Jülich: 10^6 n $cm^{-2} s^{-1}$, high flux reactor and position sensitive detector D1B at ILL Grenoble: $1.5 \cdot 10^6$ n $cm^2 s^{-1}$, pulsed source at IPNS Argonne National Laboratory: $2 \cdot 10^6$ n $cm^{-2} s^{-1}$). After diffraction and an additional 0.25 to 0.50 m path, neutrons are recorded by a Borkowski–Kopp type (1978) 2D-position sensitive 3-He gas proportional counter with an active area of 25×25 cm and a resolution of 2.5 mm (Fig. 6). The short pulse length ensures the capability of very good wavelength resolution. This geometry, with the detector set at 25 cm from the sample, covers a 2Θ range of $90° \pm 28°$ and an angular range in reciprocal space of about 40° in χ and ω. Neutron event locations are digitized with respect to the two spatial coordinates and the time-of-flight (TOF) information is appended, resulting in an array of 64 detector divisions along X and Y and 188 time frames of adjustable width. Such a $64 \times 64 \times 188$ data set is

called a histogram. The TOF t is directly proportional to the wavelength λ using the quantum relation

$$\lambda_1^{(\text{Å})} = \frac{h}{m \cdot V} = \frac{h}{m} \cdot \frac{t}{L} = 3.95 \cdot 10^{-3} \frac{t(s)}{L(m)}, \tag{1}$$

where h is Planck's constant, m and v the mass and velocity of neutrons, and L the total flight path. In our case this results in a TOF of about 2 ms for 1 Å neutrons. The beam at the sample is about 6 mm in diameter. The sample needs to be fully immersed in it, which restricts its dimensions. Absorption is minimal for most materials and can be neglected. However, the spectral variation needs to be corrected for (Figure 7, solid line), and in addition it is necessary to correct for the scattering power (λ^4). A combination of the two corrections yields a rather shallow slope between 2 and 4 Å which was used in our experiments (Figure 7, dashed line). The raw data are divided by this number. Also, since data for a single pole figure are collected at different 2Θ angles and with different

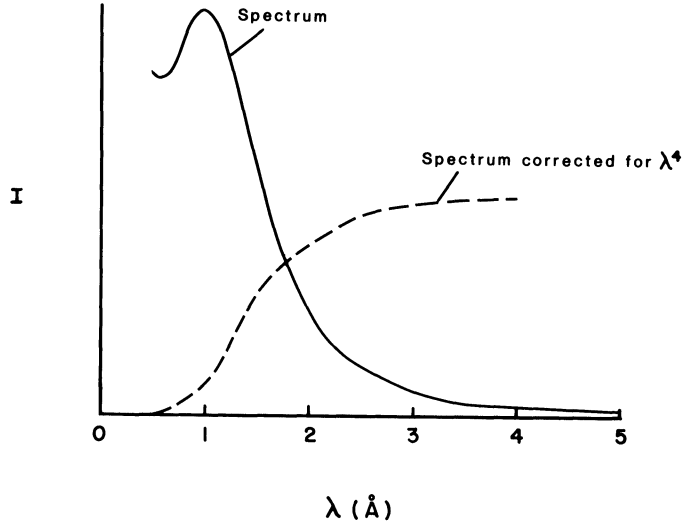

Figure 7 Spectrum of neutrons in the TOF experiments at LANSCE (solid line) and the same spectrum corrected for scattering power (dashed line). The wavelength range used in our experiments is between 2 and 4 Å.

wavelengths, a Lorentz-correction ($\sin^2 \Theta$) is necessary. After these corrections are applied, we obtain a three dimensional distribution of squared structure factors which is, within one pole figure, proportional to the volume of crystallites in a particular orientation. Details of the instrumentation are described by Vergamini *et al.* (1978).

DATA PROCESSING

The data for one sample setting are accumulated over 2 hours in 188 time frames of 64×64 arrays and stored on disk. Figure 8 illustrates a single time slice (XY) with $t = 130\,\mu$s in picket fence representation. Note the belt of high intensity which corresponds to the time intersection of the strong 111 reflection. Intensity variations along this belt are mainly due to preferred orientation. As we change time and correspondingly the wavelength, the high intensity area shifts. Notice also the very low background with many cells receiving zero neutrons. The next step is the processing by means of a Micro VAX II computer. First we project the XYT array along Y. The contoured XT diagram (Fig. 9a) displays the ridges corresponding to Bragg reflections more clearly and illustrates the

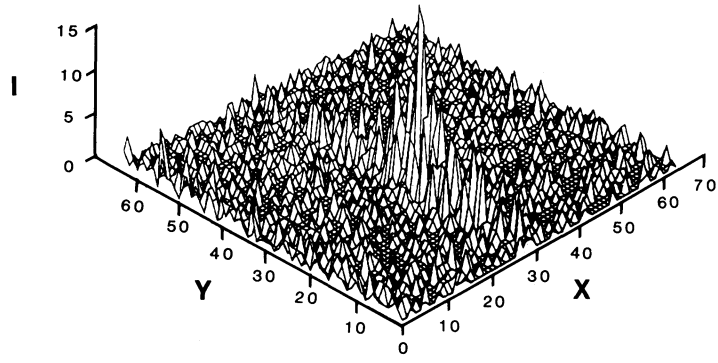

Figure 8 Timeslice of XYT histogram represented in picket fence representation. $T = 130\,\mu$s. The intensity coordinate displays number of neutrons. The high intensity range corresponds to the Bragg peak (111). The intensity variation along this range is mainly due to preferred orientation.

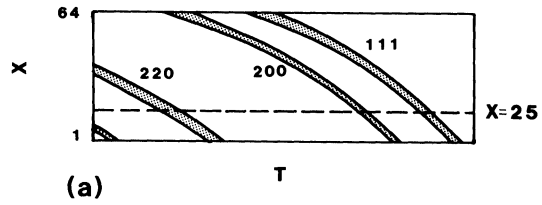

Figure 9(a) Y projection of a histogram. The contoured XT diagram displays ridges corresponding to Bragg peaks. Note that the 220 reflection is partially outside the view of the detector.

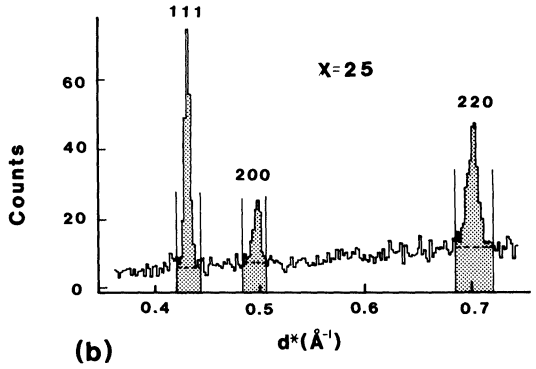

Figure 9(b) $X = 25$ slice of a histogram compressed along Y. The time coordinate is converted to d^* so that this diagram corresponds to a powder pattern and illustrates the resulution in $\Theta(d^*)$. Peaks are indexed and brackets indicate the range over which pole figures were integrated in the XYT array (shaded), background levels shown by dashed lines.

range which can be reached with the counter. Note that high X values of the 220 peak are outside the field of view and the corresponding pole figure sector is therefore limited. Subsequently we select an X slice ($X = 25$, indicated by dashed line in Figure 9a). When the intensity variation is represented in d^* coordinates (Figure 9b), this diagram corresponds more or less to a powder pattern and displays the resolution in 2Θ (d^*), which is comparable to the resolution of the D1B banana detector at ILL (Bunge *et al.* 1982, Convert 1975). We can therefore separate closely spaced peaks, an advantage which is not made use of in the analysis of an

fcc metal but is highly significant for polymers and geological specimens.

On the diagram of Figure 9 we select one diffraction peak and bracket it by a minimum and maximum d-spacing. We now integrate from d_{min} to d_{max} in the direction of the d vector over the whole XYT array, subtract the background, and correct for the spectral variations as described in the previous section. This produces for each diffraction peak hkl a two-dimensional array of integrated intensities which is contoured in Figure 10a for the 111 peak of the aluminum specimen. The diagram shows density variations due to preferred orientation of lattice planes. The XY coordinates correspond to spherical angles (Figure 3b). In Figure

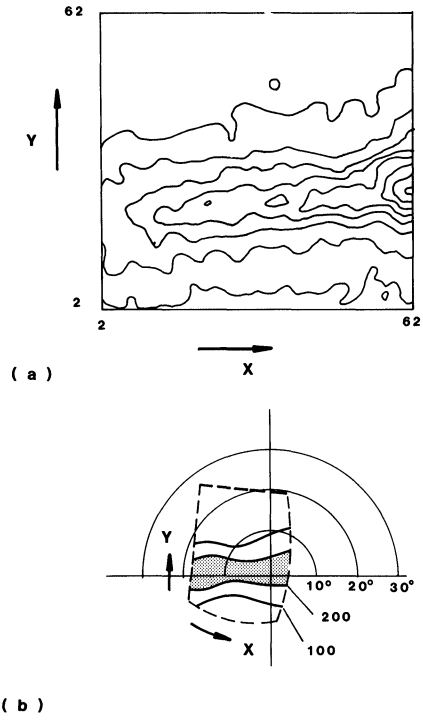

Figure 10 XY slice for a specific d interval corresponding to the 111 peak of aluminum for one sample-detector setting. (a) Cartesian XY coordinates. (b) Equal area projection relative to sample coordinates (incomplete pole figure).

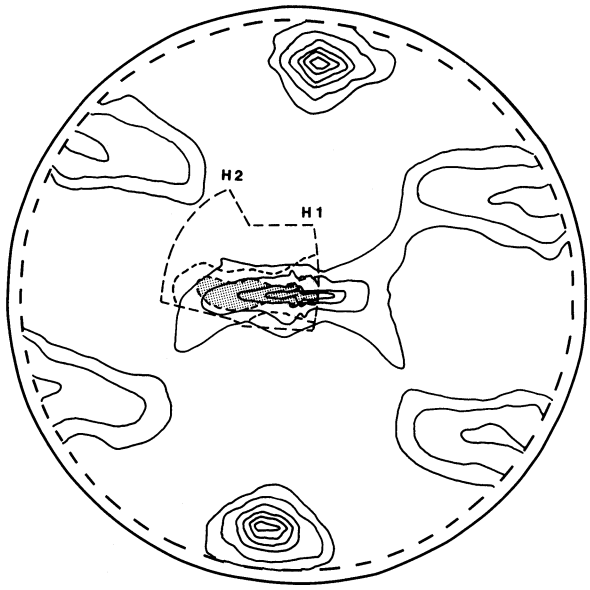

Figure 11 (222) pole figure of rolled aluminum 7039 determined by X-ray diffraction. Contours with solid lines are 1, 2, 4, 6, 8, 10 m.r.d. Superposed are TOF results from two sample/detector settings (histograms H1 and H2) shown within dashed lines. Contours of 100 and 200 arbitrary intensity units are dashed, shaded above 200. Equal area projection.

10b, the Cartesian array is represented on the sphere and plotted in equal area projection, which constitutes an incomplete pole figure.

The same procedure was undertaken for a second detector setting, thus covering a different area on the pole figure. Results from the first and second setting for the 111 pole figure are combined in Figure 11. For this pilot experiment we had insufficient beam time to cover the complete pole figure, but the good match in the region of overlap demonstrates feasibility. Also, the incomplete neutron pole figure compares well with an X-ray reflection pole figure on the same sample.

DISCUSSION

We report a first application of TOF analysis of spallation neutrons with a 2D position sensitive detector to texture analysis of deformed

polycrystals. We demonstrate feasibility with pilot experiments on a sample of recrystallized aluminum. This sample was chosen because of its well-known texture, the high diffraction intensity which was particularly significant in the early stages of this project when the storage ring was not yet available and beam intensity was low. We believe that the most interesting and most efficient use of this experiment is not in metallurgy but for materials with closely spaced diffraction peaks such as geological samples. Many pole figures can be recorded on these at once, and the orientation distribution could more or less be recorded on line, which is particularly attractive for in situ heating or deformation experiments.

At present we use the instrument as designed for single crystal experiments. It could be considerably improved for texture experiments, for example by employing a larger beam with a bigger sample and by placing the detector closer to the sample and thus covering a larger angular range, sacrificing unnecessary angular resolution. It would be optimal to construct a spherical or cylindrical detector and thus record many *complete* pole figures simultaneously. In the meantime, several measurements are necessary, or else they have to be computed from recently advanced methods of pole figures inversions (Matthies 1982). The experiment is extremely simple, and data reduction is straightforward, much easier than a crystal structure determination. Since measuring times are short (compared to single crystal data collection), it is an ideal experiment to intersperse when short beam times are available to make full use of these expensive facilities.

In this paper we have determined preferred orientation to get information about anisotropic material properties. In other experiments, such as structure determinations from powder data, texture is undesirable but often cannot be avoided. However, knowing the orientation distribution of a powder we can correct intensities for the texture anisotropy by averaging over all orientations, which is more elegant than introducing additional parameters in the structure refinement (Von Dreele *et al.*, 1982).

Acknowledgments

We are appreciative for support from the Institute of Geophysics and Planetary Physics at Los Alamos and from NSF grant EAR 84-06070 and by the Department of Energy, Basic Energy Sciences.

References

Betzl, M., Drechsler, L. P., Feldmann, K., Fuentes, L., Hennig, K., Kleinstück, K. H., Matthies, S., Matz, W., Tobisch, J., and Walther, K. (1984) *Proc. 7th Inter. Conf. on Textures of Materials, Holland,* 753–758.

Betzl, M., Kleinstück, K. (1961) *Kernenergie* **4,** 923

Borkowski, C. J., Kopp, M. K. (1978) *J. Appl. Crystall.* **11,** 430–434.

Brockhouse, B. N. (1953) *Canad. J. Phys.* **31,** 339–355.

Bunge, H. J., Wenk, H. R., and Pannetier, J. (1982) *Textures and Microstructures* **5,** 153–170.

Convert, P. (1975) Thèse d'Etat, Université de Grenoble.

Feldmann, K., Betzl, M., Andreef, A., Hennig, K., Kleinstück, K., and Matz, W. (1980) *Texture of Crystalline Solids* **4,** 1–11.

Matthies, S. (1982) *Aktuelle Probleme der quantitativen Texturanalyse.* Zentralinstitut für Kernforschung Rossendorf, Dresden, DDR.

Russell, G. J., Meier, M. M., Robinson, H., and Taylor, A. D. (1981) *Proc 5th Meeting Int. Collaboration of Advanced Neutron Sources,* Jülich, 389.

Vergamini, P. J., Christoph, G. G., Alkire, R. W., and Larson, A. C. (1987) *Nuclear Instr. Methods in Phys. Res.* (in press).

Von Dreele, R. B., Jorgensen, J. D., and Windsor, C. G. (1982) *J. Appl. Crystall.* **15,** 581–589.

Wenk, H. R., Bunge, H. J., Jansen, E., and Pannetier, J. (1986) *Tectonophysics* **126,** 271–284.

Wenk, H. R., Kern, H., Schaeffer, H., Will, G. (1984) *J. Struct. Geology* **6,** 687–692.